Cr- and Ce-Doped Ferrite Catalysts for the High Temperature Water−Gas Shift Reaction: TPR and Mossbauer Spectroscopic Study†

Gunugunuri K. Reddy,‡ Kapila Gunasekara,§ P. Boolchand,*,§ and Panagiotis G. Smirniotis*,‡

Department of Chemical and Materials Engineering and Department of Electrical and Computer Science Engineering, University of Cincinnati, Cincinnati, Ohio 45221

Received: April 1, 2010; Revised Manuscript Received: August 7, 2010

Cr and Ce-doped Fe_2O_3 catalysts are investigated for high temperature water gas shift (WGS) reaction. The chosen doping atomic ratios of Fe/metal for this investigation ranged from 10:0.2 to 10:2.5. Precipitation of Fe(III) nitrates with Cr- or Ce-metal nitrate(s) at different concentrations resulted in formation of high surface area nanosized catalysts. The WGS reaction was carried out in a fixed bed reactor at 400 and 500 °C and at atmospheric total pressure. Of all catalysts tested, Fe/Cr (10:0.5) and Fe/Ce (10:2) exhibited the highest activity within the specified activation conditions. X-ray diffraction (XRD) measurements revealed the formation of hematite (Fe_2O_3) phase in fresh catalysts, and magnetite (Fe_3O_4) phase in the activated and used catalysts after the WGS reaction. Lattice parameters reveal that the dopant ions enter the hematite structure under the present synthesis conditions. A lattice expansion occurs in the case of the Fe/Ce catalysts while a lattice contraction for the Fe/Cr catalysts. Temperature programmed reduction measurements suggest that the addition of Cr to hematite increases the transformation temperature, T_{max} of $Fe_2O_3 \rightarrow Fe_3O_4$, whereas the addition of Ce decreases T_{max} of $Fe_2O_3 \rightarrow Fe_3O_4$ transformation. Mössbauer spectroscopy studies show changes in internal magnetic field at iron octahedral sites with characteristic isomer shift "δ" resulting due to lattice contraction or expansion of the hematitic phase. These effects strongly depend on the nature and the amount of the incorporated metal cation. Mössbauer spectroscopy measurements also reveal that a rearrangement of Fe^{2+} and Fe^{3+} ions occurs between the octahedral (O_h) and tetrahedral (T_d) sites during the WGS reaction of pure Fe_2O_3. No such rearrangement was noted in the doped catalysts except for the Fe/Cr (10:0.2) case.

1. Introduction

Production of H_2 using membrane reactors via high temperature water gas shift (WGS) reaction has received much importance in recent years because hydrogen can selectively permeate through a membrane, thus making complete conversion possible. In this manner, the broad consequences of complete conversion can be explored.[1] A membrane for this reaction typically operates at temperatures of 450−550 °C and pressures ranging from 1 to 20 bar.[2−5] Development of catalysts for membrane reactors operating at these high pressures and temperatures have to meet stringent requirements.

In previous studies, we introduced a variety of metal dopants (M = Cr, Mn, Co, Ni, Cu, Zn, and Ce) for iron oxide (spinel lattice) and screened their effectiveness for high-temperature WGS reactions.[6] Among the various catalysts tested, Fe/Ce and Fe/Cr spinels exhibited the highest activity with the atomic ratio of 10:1. The idea was to examine if ferrite formation can occur with dopants and promote the $Fe^{3+} \leftrightarrow Fe^{2+}$ redox couple. The substitution of "Fe" sites in the ferrite structure with other transition/nontransition/inner transition metal atoms leads to the crystallization of an inverse (or mixed) spinel. The stoichiometry of an inverse spinel can be represented as $A_{(1-\delta)}B_{\delta}[A_{\delta}B_{(2-\delta)}]O_4$, where δ is the degree of inversion, while A and B represent typical divalent and trivalent cations, respectively.[7,8] Such introduction is expected to strongly modify the redox properties of the doped ferrites. The physical and chemical properties of ferrites are strongly dependent on the site, nature, and ion size of substituents present at A and B sites in the structure.[9,10] Furthermore, the amount of dopant can also significantly influence the covalency effect, which is of primary interest in this study.

In the present study we aim to find the optimum amount of Cr and Ce dopant that can be incorporated into the hematite lattice to promote maximum WGS activity. For this purpose, various Fe/Cr and Fe/Ce catalysts were prepared by ammonia assisted coprecipitation method with variable Fe/M (M = Cr and Ce) atomic ratios. The chosen atomic ratios for the Fe/Cr catalysts are 10:0.2, 10:0.5, 10:1, and 10:2 and for the Fe/Ce catalysts are 10:0.5, 10:1, 10:2, and 10:2.5. The as synthesized catalysts were evaluated for the high temperature WGS reaction. The WGS operating conditions were chosen to mimic conditions found in a membrane reactor. The structural and surface properties and catalytic performance of Cr and Ce doped Fe_2O_3 catalysts depend on the nature and the amount of dopant that is incorporated into the hematite lattice. The experiments were conducted at temperatures of 400 and 500 °C. For the sake of comparison, characterization and catalytic activity results of pure Fe_2O_3 were also measured. The WGS activity observed was found to be determined by the nature and amount of dopant used in a given case. Of the various Fe/Cr catalysts, the Fe/Cr (10:0.5) exhibited highest activity, whereas for the Fe/Ce catalysts Fe/Ce (10:2) exhibited better activity. Surface characterization measurements suggest that both Cr and Ce act as structural stabilizers for the magnetite during the WGS

† Part of the "Alfons Baiker Festschrift".

* Corresponding authors. Tel.: +1 513 556 1474. Fax: +1 513 556 3473. E-mail: panagiotis.smirniotis@uc.edu (P.G.S.); boolchp@ucmail.uc.edu (P.B.).

‡ Department of Chemical and Materials Engineering.

§ Department of Electrical and Computer Science Engineering.

10.1021/jp102959p
Published on Web 10/06/2010

reaction. A plausible explanation for the WGS activity over these Cr and Ce doped ferrites is proposed with the help of local and extended range structure available from Mossbauer and XRD measurements, respectively.

2. Experimental Section

2.1. Catalyst Preparation. Ammonia assisted coprecipitation route is explored for high-yield preparations of various modified spinels Fe/M (M = Ce, Cr) at different iron to metal ratios. Iron nitrate, chromium nitrate and cerium nitrate was chosen as precursors. In a typical preparation, calculated amounts of iron nitrates and the corresponding dopant metal nitrate were dissolved separately in deionized water and mixed together. Dilute aqueous ammonia was added gradually dropwise to the aforementioned mixture solutions, with vigorous stirring, until precipitation was complete (pH ~8.5). The supernatant liquid was analyzed for nitrate ions by adding about 1 mL of concentrated sulfuric acid to 10 mL of the supernatant, while the formation of $[Fe(NO)]^{2+}$ can be detected by a brown ring.[11] In our experiments the brown ring was not observed in all cases. Thus obtained precipitate gels were further aged overnight, and filtered off. The obtained cakes were oven-dried at 80 °C for 12 h and finally calcined at 500 °C for 3 h in inert environment. The rate of heating as well as cooling was always maintained at 5 °C min^{-1}. It is notable that all catalysts reported here are prepared by completely analogous procedures, which is necessary to allow direct comparison of their catalytic properties.[12]

2.2. Catalyst Characterization. ***2.2.1. Surface Area and Pore Size Distribution Analysis.*** The BET surface areas were obtained by N_2 adsorption on a Micromeritics Gemini 2360 Instrument. Prior to analysis, samples were oven-dried at 120 °C for 12 h and flushed with Argon for 2 h. The pore size distribution analyses were conducted by N_2 physisorption at liquid N_2 temperature using Micromeritics ASAP 2010 apparatus. All samples were degassed at 300 °C under vacuum before analysis.

2.2.2. X-ray Diffraction Measurements. Powder X-ray diffraction (XRD) patterns were recorded on a Phillips Xpert diffractometer using a nickel-filtered Cu Kα (0.154056 nm) radiation source. The intensity data were collected in the $3 < 2\theta < 80°$ range using 0.02° step size and a counting time of 1 s per point. Crystalline phases were identified by comparison with the reference data from ICDD files. The average crystallite size of CeO_2 was estimated with the help of the Debye−Scherrer equation, using the XRD data of all prominent lines.[13] Lattice parameter estimations were estimated by employing standard indexation methods using the intensity of high 2θ peaks (214) and (300).[13−15]

2.2.3. TPR Measurements. The temperature-programmed reduction (TPR) with hydrogen, of various catalyst samples were performed by means of an automated catalyst characterization system (Micromeritics, model AutoChem II 2920), which incorporates a thermal conductivity detector (TCD). The experiments were carried out at a heating rate of 5 °C/min. The reactive gas composition was H_2 (10 vol. %) in argon. The flow rate was fixed at 10 mL/min (STP). The total reactive gas consumption during TPR analysis was measured. The TPR measurements were carried out following activation after cooling the sample in helium flow to 50 °C. The sample was then held at 50 °C under flowing helium to remove the remaining adsorbed oxygen until the TCD signal returned to the baseline. Subsequently, the TPR experiments were performed up to a temperature of 800 °C. The water formed during the reduction was removed by using a trapper. The gas stream coming from the reactor was passed through a trapper before the gas entered into the G.C. A mixture of isopropanol and liquid nitrogen was used in the trapper to trap the formed water during the TPR experiment.

2.2.4. Mössbauer Spectroscopy. ^{57}Fe Mössbauer spectra were recorded in a transmission geometry using a constant acceleration spectrometer with liquid helium metal dewar.[16] Experiments were performed either at room temperature or at −195 °C. A 20 mCi of ^{57}Co (Rh) was used as an emitter and the spectrometer was calibrated using a α-Fe foil, and taking the isomer shift of Rh at −0.15 mm sec^{-1} wrt α-Fe. Linewidths, on the inner two lines of α-Fe were typically found to be 0.22 mm/s. An 80 mg quantity of the oxide catalyst as a fine powder was spread on a thin Teflon sheet using GE varnish as a binder, and used as an absorber. Typical run lasted 48 h and baseline counts per channel were two millions. Mossbauer spectroscopy of activated and used catalysts after the WGS reaction was also measured. The catalyst was mixed with GE varnish in nitrogen hood to prevent hydrolysis from ambient air. Line shapes were least-squares fit to a superposition of appropriate set of singlets and doublets to extract the hyperfine structure parameters hyperfine field (H), qudrapole splitting (Δ), and isomer shift (δ), and these data appear in Tables 4 and 5.

2.3. Catalyst Activity. The WGS reaction was carried out in a vertical down flow fixed bed differential ceramic microreactor (i.d. 0.635 cm) at atmospheric pressure. In a typical experiment, ca. 0.1 g of powdered catalyst was placed between two plugs of quartz wool. The reactor was placed vertically inside a programmable tubular furnace (Lindberg), which was heated electrically. The catalyst pretreatment involves the partial reduction of hematite (Fe_2O_3) to magnetite (Fe_3O_4) using a Process gas (process gas is a mixture of H_2, CO, CO_2 (99.9% pure gases), and water vapor)[17−19] with an reductant to oxidant ratio of 1.4. Prior to the reaction, the catalyst was pretreated in flowing process gas at 400 °C for 4 h. It is important to avoid over-reduction of the magnetite active phase to lower carbides, oxides, or metallic iron phases. Metallic iron phases are active catalysts for methanation and Fischer−Tropsch processes.[17] The rate of heating and cooling was always maintained at 5 °C min^{-1}. The gas flows were regulated through precalibrated mass flow controllers with digital read-out unit (MKS instruments). Water was injected into the system through a motorized syringe pump (Cole-Parmer type 74900) to generate steam. The entire system was kept at 200 °C by using heating tapes. Before pretreatment the reactor setup was flushed with an inert gas, and the pretreatment gas mixture was initialized only after the catalytic system had attained ≥150 °C. The experiments were performed at 400 and 500 °C using a constant steam to CO ratio of 3.5. The gas hourly space velocity of 60 000 h^{-1} was maintained in all of the experiments. The product stream coming from the reactor was passed through ice cooled trap to condense water, after which, the product gases were analyzed with an online TCD (Gow Mac series 550 thermal conductivity detector) having a porapak Q column for separation of the gases. This TCD was interfaced to a personal computer using a peak simple chromatography data system. The post analyses of results were done on the peak simple 2.31 software. The product-gas was injected through a six port valve, sampling was performed every 20 min interval. Reported values of conversions correspond to steady-state values at 0.5 h on stream.

3. Results and Discussion

3.1. WGS Activity. A high temperature WGS reaction has been carried out over various Fe/Cr and Fe/Ce catalysts. All of the present results were reproduced twice within the limits of permissible error. Before performing the WGS reaction, the

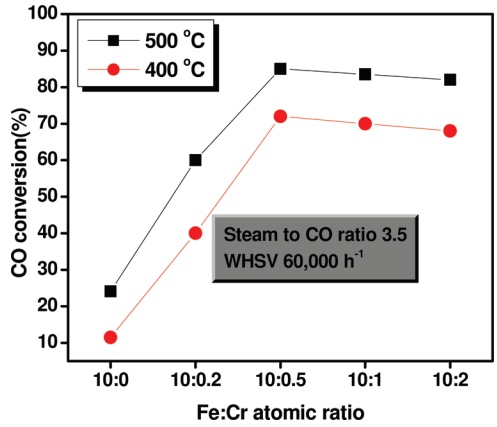

Figure 1. WGS activity results of Fe/Cr catalysts at temperatures 400 and 500 °C (WHSV = 60 000 h^{-1}, steam to CO ratio 3.5).

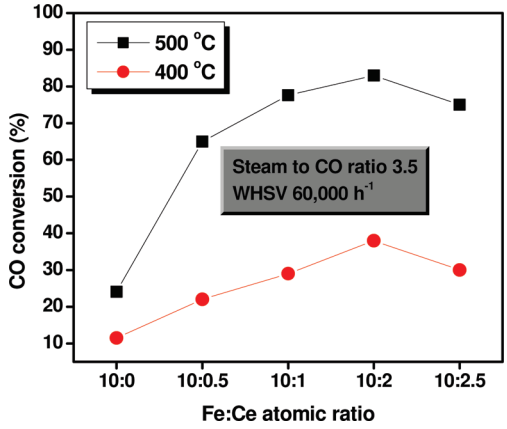

Figure 2. WGS activity results of Fe/Ce catalysts at temperatures 400 and 500 °C (WHSV = 60 000 h^{-1}, steam to CO ratio 3.5).

prepared catalysts which are in hematitic form have to be activated to magnetite form by controlled reduction in a stream of process gas such as CO, CO_2, H_2, and H_2O vapor. The ratios of water vapor to hydrogen and CO_2 to CO for the activation step determine the equilibrium of the Fe^{2+} and Fe^{3+} ions in octahedral sites. With commonly used process gases the catalyst is more reduced than the reduction to reach the state of equilibrium. In this way more Fe_3O_4 is created, which forms the stable state. It is important to avoid over reduction of the magnetite active material during the process to lower oxides, carbides, or metallic iron species. The metallic iron species especially are active catalysts for the Fischer−Tropsch process thus leading to methanation in the WGS reaction.[20] Hence, in the present study all the catalysts were activated by carrying controlled reduction of hematite to magnetite in the presence of a process gas (CO, CO_2, H_2, and steam). XRD powder diffraction patterns of all the activated catalysts show only peaks due to the magnetite phase.

The WGS activity results of Fe/Cr- and Fe/Ce-based catalysts are presented in Figures 1 and 2, respectively, at two temperatures. In this study, WGS reaction was performed at a constant steam to CO ratio 3.5. A relatively high space velocity of 60 000 h^{-1} was maintained in all of the experiments. The WGS reaction was performed at temperatures 400 and 500 °C. The reported conversion values are taken once the reaction reached steady-state. In general with increasing temperature from 400 to 500 °C, the WGS activity was found to increase. No pressure drop across the catalyst bed was observed during the experiments nor was CH_4 detected in the effluent stream. The WGS activity increased with the increasing amount of chromium up to Fe/Cr atomic ratio of 10:0.5, while further increase in the amount of chromium resulted in a slight decrease in the WGS activity. As per the literature reports the optimum atomic ratio for the Fe/Cr catalysts is 10:1 for the WGS reaction at higher reaction temperatures.[21] The interesting behavior of chromium in the present study is probably due to the different activation and preparation conditions employed. We explained this different behavior of chromium based on the various characterization techniques like Mössbauer and XRD. On the other hand, the order of WGS activity for the Fe/Ce catalysts is Fe_2O_3 < Fe/Ce (10:0.5) < Fe/Ce (10:1) < Fe/Ce (10:2) > Fe/Ce (10:2.5). Interestingly, both iron and ceria possess highly facile $Fe^{III} \leftrightarrow Fe^{II}$ and $Ce^{IV} \leftrightarrow Ce^{III}$ redox couples, respectively; the interaction between these two couples is responsible for the improved WGS activity. Additionally, the rapid increase in WGS activity with increase in reaction temperature from 400 to 500 °C is due to the improvement in the OSC of ceria at higher reaction temperatures.[22]

3.2. Structural and Surface Properties. BET surface area and pore size distribution analyses were performed over various Fe/Cr and Fe/Ce catalysts along with pure Fe_2O_3 and the corresponding results are shown in Table 1. It is clear from those data that all the Cr and Ce doped Fe_2O_3 catalysts exhibit higher surface area compared to pure Fe_2O_3. It is also evident from Table 1 that the surface area of the dopant oxide depends on the type of dopant as well as the amount of dopant. The efficacy of the dopant ion in modifying the resultant surface area could be directly related to variations in the rate of crystal growth. The nature and amount of the foreign cations present in the system govern this variation. Between the two dopants Cr and Ce, the Fe/Ce catalysts exhibit higher surface areas

TABLE 1: BET Surface Area, Crystallite Size, Cell Parameter, and Cell Volume Values of Various Fe/Cr and Fe/Ce Fresh Catalysts

sample	BET surface area (m^2/g)	crystallite size (nm)	"a" cell parameter (Å) Γ[a]	"c" cell parameter (Å) Γ[a]	cell volume (Å^3) Γ[a]
Fe_2O_3	36	34.3	5.044	13.68	301.6
Fe/Cr(10:0.2)	66	26	5.042	13.68	301.1
Fe/Cr(10:0.5)	88	13	5.039	13.67	300.7
Fe/Cr(10:1)	84	15	5.037	13.66	300.3
Fe/Cr(10:2)	78	16	5.035	13.64	299.6
Fe/Ce(10:0.5)	98	12	5.048	13.69	302.3
Fe/Ce(10:1)	109	9	5.049	13.71	302.8
Fe/Ce(10:2)	119	6.2	5.05	13.78	304.5
Fe/Ce(10:2.5)	103	11	5.05	13.79	304.8

[a] Calculated following standard indexation procedures from the peaks (300) and (214).

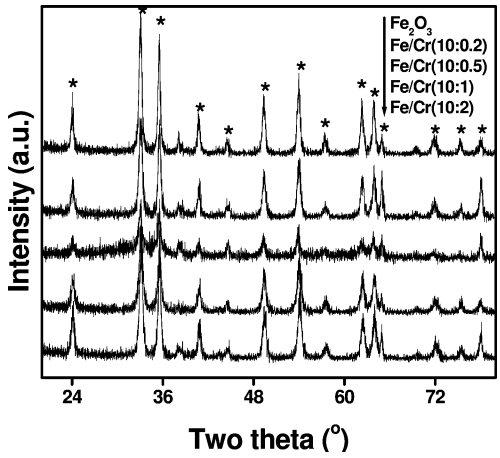

Figure 3. X-ray powder diffraction patterns of Fe_2O_3 and Fe/Cr fresh catalysts (*−Fe_2O_3).

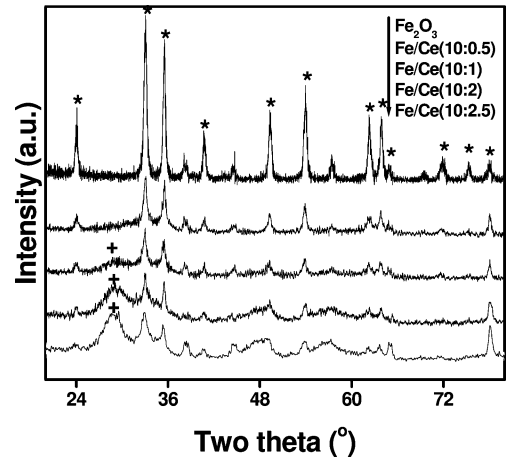

Figure 4. X-ray powder diffraction patterns of Fe_2O_3 and Fe/Ce fresh catalysts (*−Fe_2O_3, $^+$−CeO_2).

compared to the Cr doped samples. Among the various Fe/Cr catalysts, the surface area of the catalysts increases when we go from pure Fe_2O_3 to Fe/Cr (10:0.2) then to Fe/Cr (10:0.5) while further increase in the amount of Cr leads to a slight decrease in the surface area. The slight decrease in the surface area may be due to the blockage of pores of the hematite lattice by the Cr oxide particles. On the other hand in case of the Fe/Ce catalysts, the surface area increases up to the Fe/Ce atomic ratio of 10:2, while further increase in the amount of cerium leads to decrease in the surface area. A broad particle size distribution in the range of 7.0−25 nm was observed for all the investigated samples.

The as-prepared, activated, and spent Cr- and Ce-doped hematite catalysts after the WGS reaction were studied by XRD to analyze their composition and phase purity. Figure 3 shows the XRD patterns of as the prepared Fe/Cr catalysts along with the pattern of Fe_2O_3. Interestingly, all of the Fe/Cr samples exhibit intense and similar types of XRD patterns. Well resolved peaks in XRD pattern clearly indicate the polycrystalline and monophasic nature of the samples. The existence of Fe_2O_3 type phase (PDF-ICDD 33−0664) was identified by comparison with standard reference data from the PDF database. The powder diffraction analyses indicate the presence of the pure hematite crystalline phase with the reflections (012), (104), (110), (113), (024), (116), (214), and (300).[23] The observation of hematite phase in all of the catalysts is of significant importance in the present investigation since during the catalyst activation the hematite phase is converted to the magnetite phase (Fe_3O_4), which is the active phase for the WGS reaction. Additionally, the XRD spectra for the Cr modified ferrite samples do not show any extra crystalline phases due to either chromium or compounds between chromium and iron. On the other hand, X-ray powder diffraction patterns of Fe/Ce catalysts are amorphous (Figure 4) and exhibited poor diffraction lines due to hematitic phase. In addition to these lines, a peak at $2\theta = 30°$ was observed for the Fe/Ce catalysts expect for Fe/Ce (10:0.5) sample. The intensity of this peak increases with increasing the amount of cerium. This peak is due to the reflections from (111) plane of the CeO_2 phase.[24]

Figures 5 and 6 show the X-ray diffraction patterns of the various Fe/Cr and Fe/Ce activated catalysts. All of the patterns confirmed the existence of Fe_3O_4 (Magnetite) phase. Magnetite (Fe_3O_4) crystallizes in a cubic inverse spinel structure [AB_2O_4 type] at RT, where 1/3 of the Fe ions occupy tetrahedrally coordinated A sites as Fe^{3+} and the remaining 2/3 of the Fe ions having equal numbers of Fe^{2+} and Fe^{3+} are located on

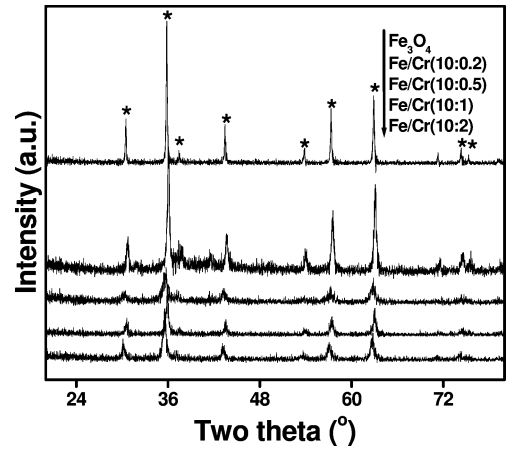

Figure 5. X-ray powder diffraction patterns of Fe_2O_3 and Fe/Cr activated catalysts (*−Fe_2O_3).

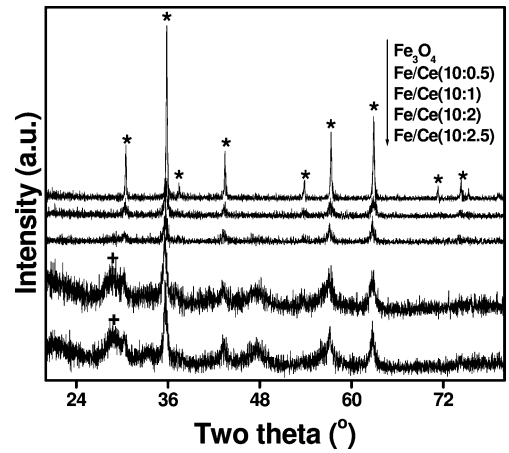

Figure 6. X-ray powder diffraction patterns of Fe_2O_3 and Fe/Ce activated catalysts (*−Fe_2O_3, $^+$−CeO_2).

octahedrally coordinated B sites. It is a well established fact that rapid electron hoping between $Fe^{2+} \leftrightarrow Fe^{3+}$ in the Fe_3O_4 lattice system is needed for carrying out the water gas shift reaction.[25] Peaks due to the ceria were also observed in the Fe/Ce activated catalysts except for the Fe/Ce (10:0.5) catalyst. There are no peaks pertaining to either chromium or compound formation between iron and chromium in Fe/Cr activated catalysts. There was no evidence for the formation of Fe (metallic) or Fe_2C phases due to over reductions, which are inactive phases for the water gas shift reaction. The X-ray powder diffraction

TABLE 2: Crystallite Size, Cell Parameter, and Cell Volume Values for Various Fe/Cr and Fe/Ce Activated and Used Catalysts after the Reaction

	activated catalysts			used catalysts		
sample	crystallite size (nm)	"a" cell parameter (Å) Γ[a]	cell volume (Å^3) Γ[a]	crystallite size (nm)	"a" cell parameter (Å) Γ[a]	cell volume (Å^3) Γ[a]
Fe_3O_4	40.3	8.30	571.7	52.6	8.29	569.7
Fe/Cr(10:0.2)	32	8.3	571.7	38	8.29	569.7
Fe/Cr(10:0.5)	15	8.29	569.7	15.7	8.28	567.6
Fe/Cr(10:1)	16.7	8.28	567.6	17.5	8.28	567.6
Fe/Cr(10:2)	18	8.28	567.6	19.2	8.27	565.6
Fe/Ce(10:0.5)	18	8.32	575.9	23	8.31	573.8
Fe/Ce(10:1)	14	8.34	580.1	16	8.33	578
Fe/Ce(10:2)	9	8.35	582.2	11	8.31	573.8
Fe/Ce(10:2.5)	16	8.35	582.2	19	8.34	580.1

[a] Calculated following standard indexation procedures from the peak (311).

patterns of the used catalysts after the WGS reaction (not shown) also show peaks due to magnetite phase only. There are no peaks pertaining to either wustite (FeO) or metallic iron. These results indicate that all of the catalysts are stable in terms of composition during the reaction.

The crystallite sizes (D_{XRD}) of pure Fe_2O_3 and various Cr and Ce doped Fe_2O_3 fresh catalysts investigated in the present study are summarized in Table 1. One can observe that all of the Cr and Ce doped ferrites exhibit smaller crystallite sizes compared to the pure Fe_2O_3. The crystallization of Fe_2O_3 apparently depends on the type of the dopant introduced into its lattice and also on the amount of dopant. Between the two doped catalysts Ce doped catalysts exhibit lesser crystallite sizes compared to the Cr doped ones. Among various Fe/Cr catalysts, the crystallite size of hematite decreased with an increasing amount of chromium up to 5 wt % (Fe/Cr (10:0.5), whereas further increase in the amount of chromium resulted in increase of the crystallite size. On the other hand, the crystallite size of Fe_2O_3 decreased with the addition of cerium up to 20 wt % (Fe/Ce (10:2). Upon further doping of cerium reverse trend was observed namely the crystallite size increased. This is due to the demixing of cerium with the hematite, which leads to a separate ceria phase in bulk. The cell parameter and TPR measurements (given in later sections) also support this observation. The crystallite sizes of Fe_2O_3 in the activated catalysts are shown in Table 2. All of the activated catalysts exhibited higher crystallite size compared to the fresh catalysts. The rate of the crystallite growth is higher in the case of cerium doped catalysts compared to the chromium doped catalysts. This results conforms the fact that chromium is acting as a better stabilizing agent than cerium, although the crystallite size of cerium doped catalysts is smaller in fresh catalysts. The crystallite size of Fe_2O_3 was further increased after the water gas shift reaction. The order rate of crystallite growth in Fe/Cr catalysts is Fe_2O_3 > Fe/Cr (10:0.2) > Fe/Cr (10:0.5) ≈ Fe/Cr (10:1) ≈ Fe/Cr (10:2). On the other hand Fe/Ce catalysts exhibited a different trend, and the order is Fe_2O_3 > Fe/Ce (10:0.5) > Fe/Cr (10:1) > Fe/Cr (10:2) < Fe/Cr (10:2.5). On the whole, Fe/Cr (10:0.5) in the Cr doped samples, Fe/Ce (10:2) in the Ce doped samples exhibiting smaller crystallite size in fresh, activated, and spent catalysts.

Using the interplanar spacing values, calculation of the cell parameters was carried out for the fresh catalysts (Table 1). This revealed that all the substitutent ions enter the hematite lattice under the preparation conditions employed in this work. Experimental values of lattice constant were calculated from higher 2θ lines i.e., from (214) and (300) planes for each sample.[18] By comparing the values of the modified ferrite samples with that of the pure Fe_2O_3 sample, prepared by an identical method, it is observed that the lattice expansion is taking place in the case of Fe/Ce catalysts and lattice contraction takes place in the case of the Fe/Cr catalysts. This is due to the fact that cerium possesses larger ionic radii than Fe^{3+} thereby leading to the lattice (cell volume) expansion. On the contrary, when Cr^{3+} replaces Fe^{3+} ions from their octahedral positions, the distance between them is reduced thereby leading to the lattice (cell volume) contraction. The cell volume of hematite lattice increased up to the cerium doping amount of 20% (Fe/Ce (10:2)) and there is no change in the value of cell volume upon further addition of cerium. These results confirm that cerium can be incorporated into the hematite lattice up to the Fe/Ce atomic ratio of 10:2. XRD patterns, crystallite size and cell parameter values suggest that cerium can be incorporated into the hematite lattice up to the Fe/Ce atomic ratio 10:2 and further increase in the atomic ratio forms a separate CeO_2 phase in the bulk. On the other hand, cell volume decreased with an increasing amount of chromium. Cell parameter calculations were also made for the activated and used catalysts and the corresponding results were presented in Table 2. X-ray diffraction patterns reveal that both activated and used catalysts exhibit peaks due to the magnetite phase which is a cubic lattice. Hence, the lattice constant values are measured from the (311) plane. Cell parameter values of both activated and used catalysts follows the same trend as fresh catalysts. Lattice expansion is taking place in the case of the Fe/Ce catalysts and lattice contraction takes place in the Fe/Cr catalysts. These values also support the fact that cerium can be incorporated into the magnetite lattice up to the Fe/Ce atomic ratio 10:2. After the water gas shift reaction a large decrease in the cell volume of the magnetite lattice was observed for the pure Fe_2O_3 catalyst compared to the activated catalysts. This is due to the rearrangement of Fe ions between the O_h and T_d sites during the WGS reaction. Mossbauer spectroscopy results present in the later section also supports this observation. On the other hand, all the dopant catalysts exhibit a slight decrease in the cell volume compared to the activated catalysts except Fe/Cr (10:0.2). These results suggest that both Cr and Ce stabilize the magnetite during the WGS reaction.

3.3. TPR Measurements. The temperature programmed reduction experiments were performed in order to obtain information about reducibility of samples as well as T_{max} of phase transformations. The TPR patterns of pure Fe_2O_3, various Fe/Cr, and Fe/Ce catalysts were presented in Figures 7−9, respectively. The corresponding T_{max} values for each reduction step of iron oxide are shown in Table 3. The TPR experiments on all these samples were repeated three times to check for the reproducibility. Similar profiles were observed for all the catalyst

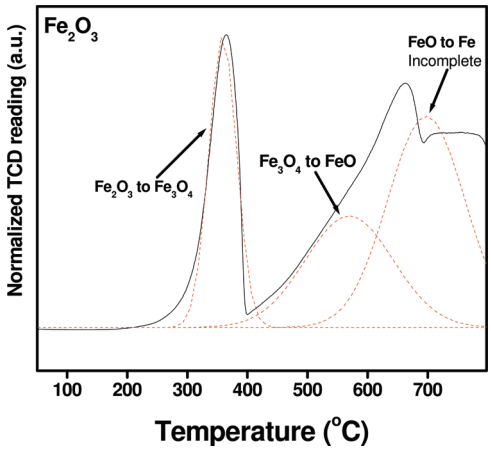

Figure 7. TPR profile of the Fe_2O_3.

samples. In the TPR of pristine hematite (Fe_2O_3), the first reduction peak appears at 356 °C, corresponding to the reductive transition of Fe_2O_3 to Fe_3O_4 [26, 27]. The peak at 565 °C corresponds to the transformation of Fe_3O_4 to FeO. Under the experimental conditions of the present study, complete reduction of FeO to metallic Fe was not observed even up to 800 °C, only partial reduction took place. Within the experimental conditions of the present study formation of metallic iron species was delayed (prolonged), which can be attributed to the method of preparation employed in this investigation.

TPR patterns of Fe/Cr catalysts are presented in Figure 8. Expect Fe/Cr (10:0.2), all of the Fe/Cr catalysts exhibited three peaks in their TPR patterns. Fe/Cr (10:0.2) exhibits 4 peaks. The first peak occurs in the temperature region 250−300 °C. This peak corresponds to the reduction of $Cr^{6+} \rightarrow Cr^{3+}$, interestingly further partial reduction of $Cr^{3+} \rightarrow Cr^{2+}$ which is expected at 490 °C[28,29] was not observed in the present study. In the Fe/Cr (10:0.2) sample this peak was observed at 249 °C and with increasing amount of chromium from the atomic ratio 10:0.2 to 10:2 this peak was shifted to higher temperature 291 °C. Reduction of $Fe_2O_3 \rightarrow Fe_3O_4$ was observed in the temperature region 380−450 °C in the Fe/Cr catalysts. In this case also a high increase in the reduction temperature was detected for the phase transformation of hematite to magnetite with increasing amount of chromium. These results reveal that chromium is acting as a structural stabilizer for the hematite. Further reduction of Fe_3O_4 to FeO occurs at higher temperatures. This reduction was completed for only the Fe/Cr (10:0.2) sample and for the remaining Cr doped catalysts this reduction was not completed. In addition to these peaks, the Fe/Cr (10:0.2) sample also exhibited a peak due to reduction of FeO to Fe. Figure 9 presents the TPR patterns of Fe/Ce catalysts. One can observe from Figure 9 all of the Fe/Ce catalysts exhibiting four peaks in their TPR patterns. The peak in the low temperature region is due to the reduction of hematite (Fe_2O_3) to magnetite (Fe_3O_4). Unlike chromium, addition of cerium to Fe_2O_3 enhancing the reducibility of hematite and the phase transformation of hematite to magnetite shifted toward lower temperatures. This could be related to the close interaction between Fe and Ce cations, which occur during the coprecipitation process. This enhancement was increased with increasing the amount of cerium up to Fe/Ce atomic ratio of 10:2 and remains constant

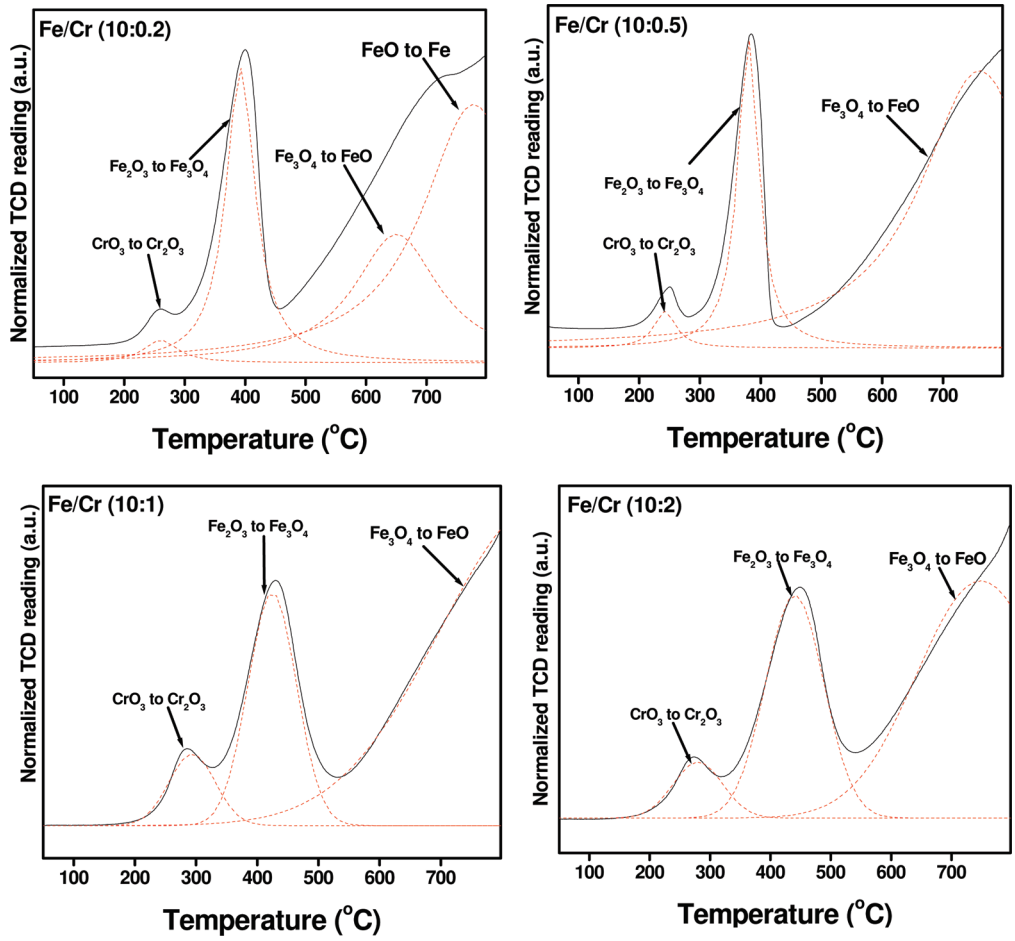

Figure 8. TPR profiles of Fe/Cr catalysts.

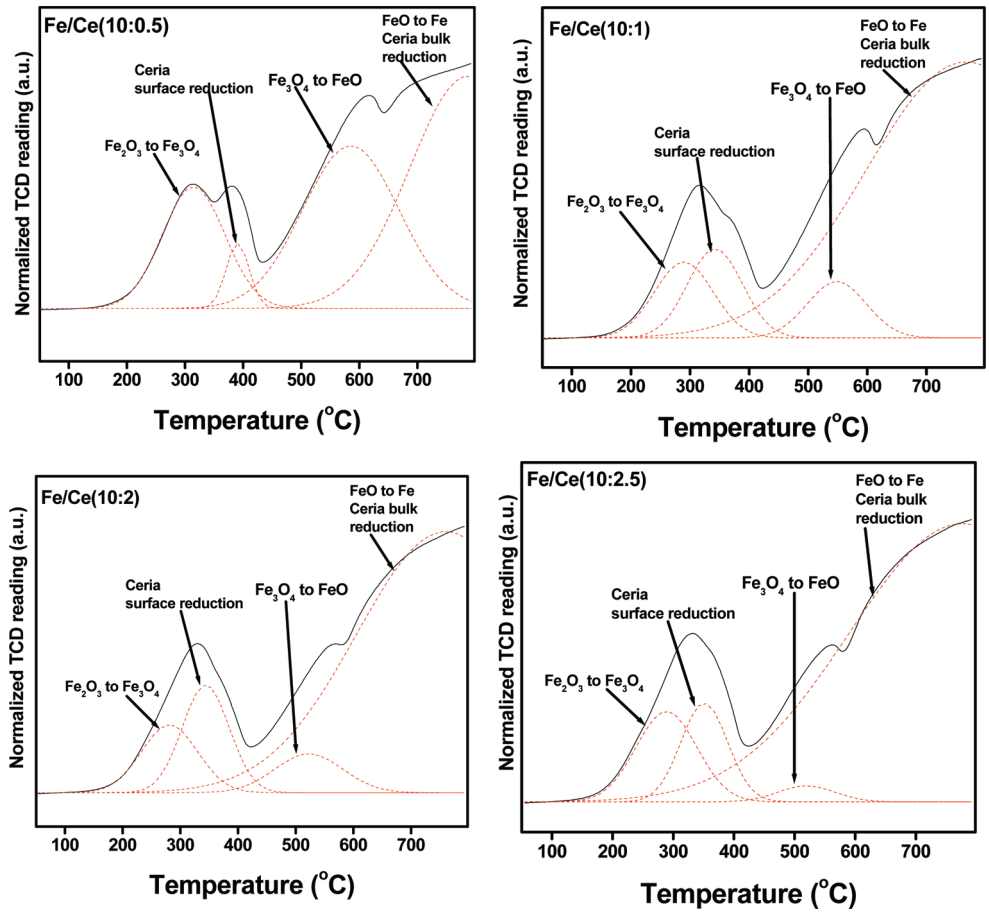

Figure 9. TPR profiles of Fe/Ce catalysts.

TABLE 3: T_{max} (°C) Values of Various Phase Transformations of the Fe/Cr and Fe/Ce Catalysts

	T_{max} (°C) of phase transformation					
sample	$Fe_2O_3 \rightarrow Fe_3O_4$	$Fe_3O_4 \rightarrow FeO$	$FeO \rightarrow Fe$	$CrO_3 \rightarrow Cr_2O_3$	surface ceria reduction	bulk ceria reduction
Fe_3O_4	356	565	>700			
Fe/Cr(10:0.2)	383	651	>700	249		
Fe/Cr(10:0.5)	400	>700	NO	261		
Fe/Cr(10:1)	429	>700	NO	275		
Fe/Cr(10:2)	447	>700	NO	291		
Fe/Ce(10:0.5)	315	575	>600		389	>600
Fe/Ce(10:1)	288	577	>600		340	>600
Fe/Ce(10:2)	275	570	>600		339	>600
Fe/Ce(10:2.5)	278	565	>600		335	>600

on further increase in the amount of cerium. This is due to the formation of separate CeO_2 phase in the bulk as evidenced by XRD and cell parameter results. The second reduction peak in the temperature region of 330−390 °C is due to the surface ceria reduction. As per literature reports, this peak occurs at 485 °C in the case of pristine ceria sample. According to Trovarelli et al.,[30] TPR trace for ceria is not controlled by the rate of diffusion of the oxygen vacancies, instead surface reduction process and the difference of both thermodynamic and kinetic properties existing in the ceria microcrystals (as a function of their size) are critical factors. The third peak due to transformation of Fe_3O_4 to FeO was observed in the temperature region of 560−580 °C. This transformation was not affected very much by the presence of cerium. Further reduction of FeO to Fe and bulk reduction of ceria was observed at higher temperatures (>600 °C). The intensity of the peak due to the surface ceria reduction increase with increasing amount of ceria up to atomic ratio 10:2 and further increase in the amount of ceria leads to the decrease in the intensity. These results suggest that most of the ceria was segregated in the bulk as a separate phase, which is in accordance with cell parameter measurements. Also in the case of Fe/Ce (10:2.5) catalyst, peak due to the bulk ceria reduction started so early compared to other samples.

3.3. Mössbauer Spectroscopy Results. To complement XRD and phase transformation with TPR, Mossbauer spectroscopic measurements performed on both activated and used catalysts after the WGS reaction. Mössbauer spectroscopy provides a powerful local probe of the Fe oxidation state in these systems. From X-ray powder diffraction data, we concluded that all the Cr- and Ce- doped activated Fe_2O_3 catalysts consist of magnetite phase (Fe_3O_4). Magnetite possesses an inverse spinel structure with oxygen ions forming a face-centered cubic close packed structure. Schematically Fe occupancy can be described as (Fe^{3+}) $[Fe^{2+}, Fe^{3+}]$ O_4 where the cation in parentheses () occupies at tetrahedral sites while one in [ ] brackets occupies octahedral lattice sites.[31] Stoichiometric magnetite has all available substitutional sites occupied by Fe^{2+} and Fe^{3+} ions. Nonstoichiometric magnetites also exist, partial

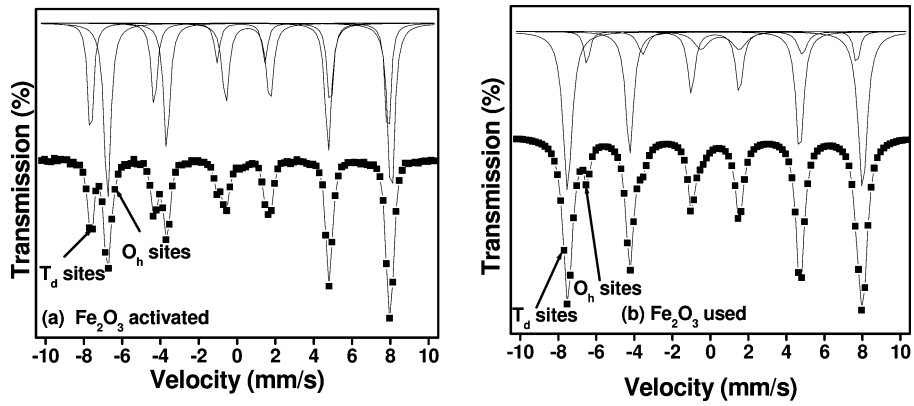

Figure 10. Room temperature Mössbauer spectroscopy data of (a) Fe_2O_3 activated (b) Fe_2O_3 used after the reaction.

TABLE 4: Isomer Shift (δ), Magnetic Field (H), Quadrapole Splitting (Δ), and Concentration Ratio of Octahedral to Tetrahedral Sites in Various Fe/Cr and Fe/Ce Activated Catalysts

	T_d sites (Fe^{3+})			O_h sites (Fe^{2+}, Fe^{3+})			
sample	δ (mm/s)[a]	H (T)	Δ (mm/s)	δ (mm/s)[a]	H (T)	Δ (mm/s)	O_h sites/T_d sites
Fe_3O_4	0.31	516.4	−0.078	0.51	493.1	0.047	1.9
Fe/Cr(10:0.2)	0.31	516	−0.07	0.50	485.1	0.061	2.06
Fe/Cr(10:0.5)	0.32	516.8	−0.033	0.48	482.3	0.023	2.09
Fe/Cr(10:1)	0.32	513.1	−0.02	0.47	475.4	0	2.51
Fe/Cr(10:2)	0.32	510.2	−0.009	0.45	453.7	−0.006	3.5
Fe/Ce(10:0.5)	0.32	510.9	−0.012	0.47	476.8	0.004	2.1
Fe/Ce(10:1)	0.33	509.3	−0.01	0.47	471.4	0.006	2.44
Fe/Ce(10:2)	0.32	508	−0.01	0.46	470.9	0.016	3.4
Fe/Ce(10:2.5)	0.32	504	−0.01	0.47	465	0.014	3.36

[a] Relative to the α-Fe.

site occupancies of base Fe- sites and impurity additives. The magnetic properties of magnetite have been broadly explained on the assumption that spins at octahedral and tetrahedral sites form two antiferromagnetically coupled sublattices.[32] In addition, stoichiometric magnetite undergoes an order−disorder phase transition at 120 K which is attributed to fast electron hopping between Fe^{2+} and Fe^{3+} octahedral cations above 120 K.[33] Associated with this transition is an anomaly in both the specific heat and electrical conductivity of magnetite. On such a picture, one might expect three different Fe sites in magnetite: one from Fe^{3+} ions at tetrahedral sites, one from the Fe^{3+} ions at octahedral sites, and another from the Fe^{2+} ions in the octahedral sites. In fact, in stoichiometric magnetite there is only two 6-line hyperfine structure.[34,35] Above 120 K these features are generally identified with Fe^{3+} ions in the tetrahedral sites, and the other with both Fe^{3+} and Fe^{2+} ions at octahedral sites, i.e. one 6-line hyperfine structure is due to all tetrahedral cations and the other due to octahedral cations. Below 120 K, however, the observed structure is identified as one 6-line spectrum coming from Fe^{3+} ions in both sites and the other from Fe^{2+} ions. The explanation for the spectral change is attributed to the electron exchange between ions at the octahedral sites, which is rapid above 120 K but shows down below that temperature.

Figure 10a shows Mossbauer spectrum of our activated pure Fe_2O_3 sample. The corresponding hyperfine structure, such as isomer shift (δ), quadrapole splitting (Δ), and magnetic field (H) are presented in Table 4. The spectra show two well-developed 6-line magnetic hyperfine structures typical of bulk materials with no trace of superparamagnetic behavior. The higher field spectrum is due to Fe^{3+} ions at tetrahedral sites (T_d), whereas the low field spectrum arises from Fe^{2+} and Fe^{3+} ions at octahedral (O_h) sites.[36] The isomer-shift and magnetic field values presented in Table 4 and are in good agreement with previous reports.[37−39] The fraction occupancy of octahedral to tetrahedral sites (O_h/T_d) is close to 2 for pure activated Fe_2O_3 catalyst (Figure 10a); there are twice as many Fe atoms at octahedral sites than at tetrahedral ones. We shall revision the discussion of how the Fe local structure changes upon WGS reaction. Mössbauer spectra of various Fe/Cr activated catalysts are presented in Figure 11. Here we also observe two 6-line hyperfine structures corresponding to the T_d and O_h sites. The δ and H values of T_d sites are similar to those in the case of pure Fe_3O_4. On the other hand, both δ and H values for O_h sites systematically decrease with chromium addition. When chromium is doped, into the Fe_2O_3, it replaces equal amounts of Fe^{2+} and Fe^{3+} ions at octahedral sites.[40] Such replacement of ions may be responsible for the decreased H-field values. The concentration ratio of O_h/T_d presented in Table 4 also supports this observation. The ratio of O_h/T_d increases with chromium alloying content into Fe_2O_3 lattice.

Figure 12 shows Mössbauer spectra of Fe/Ce activated catalysts with cerium content increasing in the sequence from panels a to d. Mössbauer spectrum of Fe/Ce (10:0.5) catalyst Figure 12a is similar to spectrum of pure Fe_3O_4 and consists of two 6-line patterns. For the remaining Fe/Ce catalysts, in addition to these two 6-line patterns, a singlet is observed at the center of the spectrum, i.e., near zero velocity. This singlet is due to the super paramagnetic behavior in the catalysts, resulting from a collapse of H-field in nanoparticles. The singlet feature is most intense in the Fe/Ce (10:2) and decreases as the Ce content either decreases or increases from the value 10:2. The crystallite size and cell parameters of hematite decrease upon cerium alloying up to Fe/Ce atomic ratio of 10:2, suggesting solid solution formation. However, a further increase in cerium content leads to the formation of a separate ceria rich phase in the bulk, suggestive of

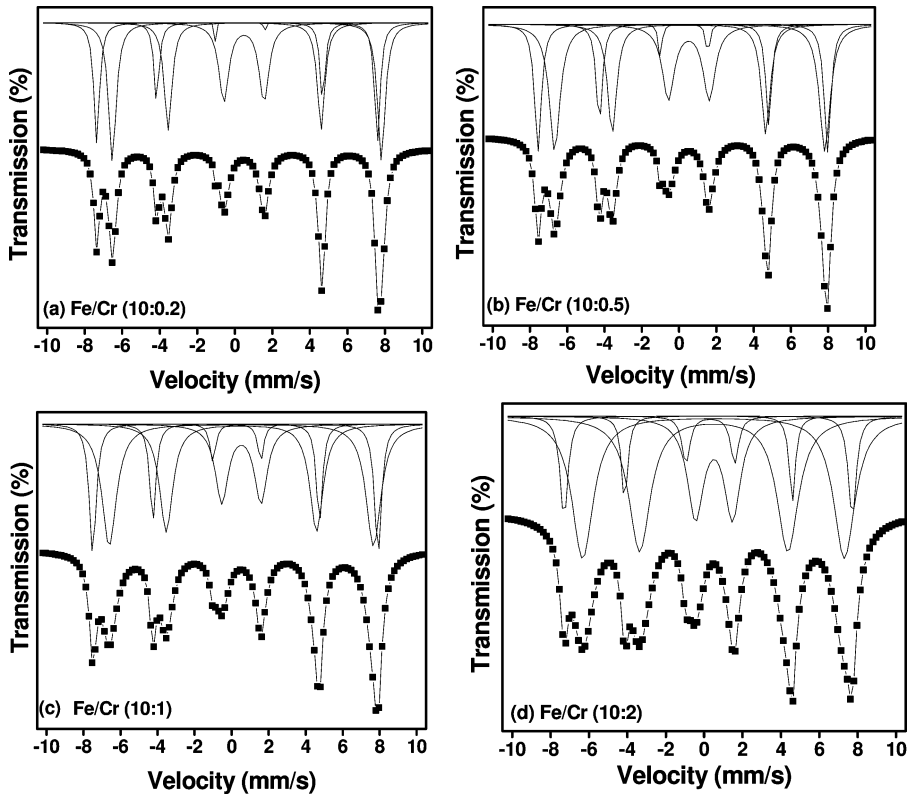

Figure 11. Room temperature Mossbauer spectroscopy data on activated Fe/Cr catalysts at indicating doping concentrations (a) Fe/Cr (10:0.2), (b) Fe/Cr (10:0.5), (c) Fe/Cr (10:1), and (d) Fe/Cr (10:2).

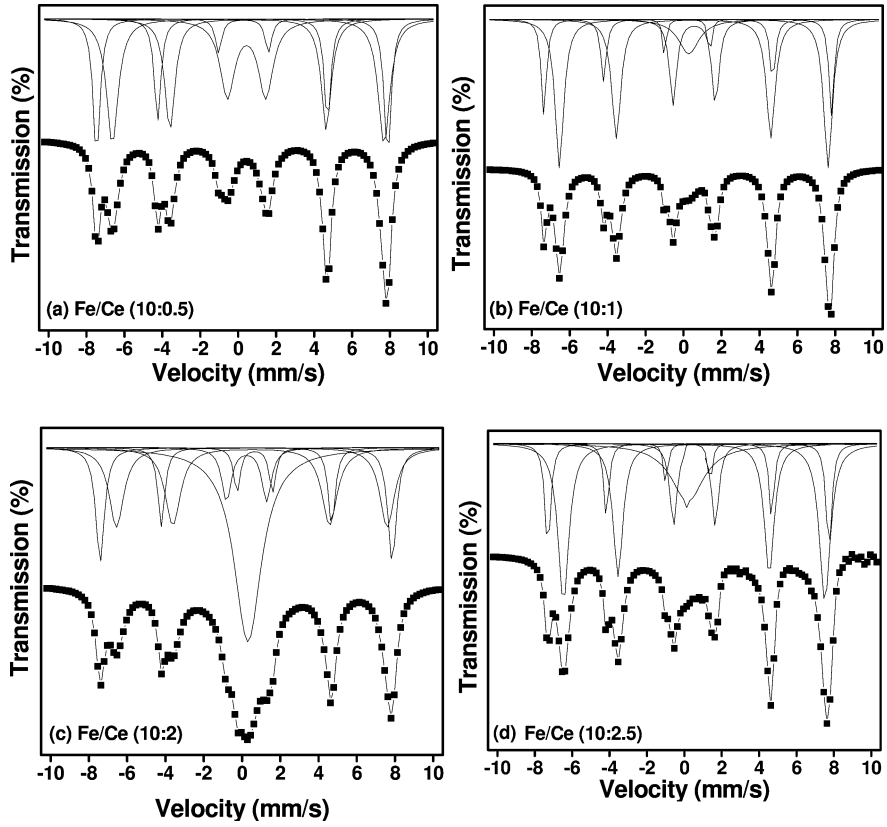

Figure 12. Room temperature Mossbauer spectroscopy data on activated Fe/Cr catalysts at indicating doping concentrations (a) Fe/Ce (10:0.5), (b) Fe/Ce (10:1), (c) Fe/Ce (10:2), and (d) Fe/Ce (10:2.5).

demixing of the additive, and such demixing leads to an increase in the crystallite size of hematite. In this manner, we can understand the higher superparamagnetic fraction observed in the Fe/Ce (10:2) sample compared to the Fe/Ce (10:2.5) sample. Like chromium, cerium also replaces Fe^{3+} and Fe^{2+} ions at octahedral sites. The hyperfine field

TABLE 5: Isomer Shift (δ), Magnetic Field (H), Quadrapole Splitting (Δ), and Concentration Ratio of Octahedral to Tetrahedral Sites in Various Fe/Cr and Fe/Ce Used Catalysts after the Reaction

	T_d sites (Fe^{3+})			O_h sites (Fe^{2+}, Fe^{3+})			
sample	δ (mm/s)[a]	H (T)	Δ (mm/s	δ (mm/s)[a]	H (T)	Δ (mm/s)	(Fe^{2+}, Fe^{3+})/(Fe^{3+})
Fe_3O_4	0.33	517	−0.011	0.52	493.1	−0.016	0.6
Fe/Cr(10:0.2)	0.33	510.6	−0.014	0.48	485.1	−0.0017	0.81
Fe/Cr(10:0.5)	0.33	509.8	−0.017	0.48	482.3	−0.0018	2.06
Fe/Cr(10:1)	0.32	506.9	−0.017	0.46	475.4	−0.007	2.45
Fe/Cr(10:2)	0.32	502.1	−0.018	0.44	453.7	−0.01	3.4
Fe/Ce(10:0.5)	0.32	508.8	−0.014	0.48	476.8	0.0072	2.05
Fe/Ce(10:1)	0.33	507.9	−0.014	0.47	471.4	0.0032	2.23
Fe/Ce(10:2)	0.32	505	−0.018	0.43	470.9	0.013	3.1
Fe/Ce(10:2.5)	0.32	504.8	−0.018	0.42	470.5	0.010	3.2

[a] Relative to the α-Fe.

parameters at octahedral sites and the O_h to T_d site fraction are presented in Table 4 and support the observation.

How does the Fe-local structure of Fe_3O_4 catalyst changes upon WGS reaction? Mössbauer spectrum of Fe_2O_3 after the WGS reaction (Figure 10b) shows remarkable change (Figure 10b). The corresponding hyperfine structure parameters are shown in Table 5. The δ and H values remain almost unchanged after the WGS reaction. However, O_h to T_d fraction reduces strikingly from 1.9 to 0.6 (see Tables 4 and 5). This is suggestive of a local structural rearrangement of Fe^{2+} and Fe^{3+} cations during the WGS reaction. The addition of a small amount of chromium, i.e., Fe/Cr (10:0.2), also reduces the O_h/T_d fraction from 2 to 0.81 (spectra not shown). On the other hand, the O_h/T_d fraction remains almost unchanged at other Fe/Cr catalysts. These results suggest that in order to stabilize the magnetite phase during the WGS reaction one needs 0.5 atoms of chromium for 10 atoms of Fe. The O_h/T_d fraction also remains unchanged at all of the Fe/Ce catalysts investigated during the WGS reaction (spectra not shown). The superparamagnetic component in the Fe/Ce (10:2) catalyst persists even after the WGS reaction, whereas at the other Fe/Ce catalysts 10:1 and 10:2.5, the feature is found to disappear. The disappearance is related to the growth in the crystallite size of magnetite during WGS reaction, which is corroborated with XRD results on crystallite size.

3.4. Structure−Activity Relationship. The simultaneous precipitation of Fe (III) nitrate with either Cr or Ce nitrates results in the formation of high surface area nanocrystalline catalysts. The overall WGS activity depends on various parameters like activation conditions, the nature of the dopant incorporated as well as the amount of doping.[41] Among the various Fe/Cr catalysts, Fe/Cr (10:0.5) shows better WGS activity compared to other catalysts. When we plot the normalized CO conversion per unit surface area as a function of Fe/Cr ratio, then all of the catalysts show equal activity. This confirms that the higher activity observed for the Fe/Cr (10:0.5) catalyst is purely due to the higher surface area. XRD and crystallite size measurements also suggest that the addition of Cr decreases the crystallite size of hematite up to the Fe/Cr (10:0.5) atomic ratio and further increase in the amount of chromium increases the crystallite size slightly. TPR results suggest that addition of Cr to Fe shifts the temperature maxima of magnetite to wustite phase to much higher temperature and stabilizes the magnetite phase during the WGS reaction. Mossbauer spectroscopic results show that in the pure magnetite, structural rearrangements of Fe^{2+} and Fe^{3+} ions take place during the WGS reaction which leads to the lower WGS activity. These rearrangements continue in Fe/Cr (10:0.2) catalyst as well. On the other hand, in other Fe/Cr catalysts with the atomic ratios 10:0.5, 10:1, and 10:2, chromium stabilizes the magnetite phase during the WGS reaction and thus leads to a higher WGS activity. A slight decrease in the WGS activity for Fe/Cr (10:1) and Fe/Cr (10:2) catalysts compared to Fe/Cr (10:0.5) might be due to the smaller BET surface area as well as larger crystallite size. The order of WGS activity for the Fe/Ce catalysts is Fe_2O_3 < Fe/Ce (10:0.5) < Fe/Ce (10:1) < Fe/Ce (10:2) > Fe/Ce (10:2.5). Cell parameter and crystallite size measurements reveal that cerium can incorporate into the hematite lattice and decrease the crystallite size by forming solid solutions. On the other hand further increase in the amount of cerium (Fe/Ce 10:2.5) leads to a separate ceria phase in the bulk and a consequent increase in the hematite crystallite size. TPR results suggest that addition of Ce to Fe shifts the temperature maxima of hematite to magnetite to lower temperatures and promotes the WGS activity. Mössbauer spectroscopic results also confirm that superparamagnetic behavior persisting even after the WGS reaction for Fe/Ce (10:2), whereas for the other two catalysts, i.e., Fe/Ce (10:1) and Fe/Ce (10:2.5), one observes a loss in the superparamagnetic fraction. Superior superparamagnetic behavior and extreme nanoparticle nature may be responsible for the higher WGS activity, as observed for the case of Fe/Ce (10:2) catalyst. The formation of separate ceria phase in the bulk decreases the WGS activity for Fe/Ce (10:2.5) catalyst. On the whole the optimum atomic ratio for the Fe/Cr catalyst is 10:0.5 and for the Fe/Ce is 10:2 within the present preparation and activation conditions.

4. Conclusions

In the present study we have synthesized Cr- and Ce-doped hematite catalysts. After activation in a controlled atmosphere hematite turns into the magnetite phase. High temperature WGS reactions were performed over these activated systems as a function of dopant concentration. The fresh, activated, and spent catalysts were characterized by XRD, TPR, and Mössbauer spectroscopic techniques. Our results show that of the catalyst examined the Fe/Cr (10:0.5) and Fe/Ce (10:2) catalysts are the best catalysts for the WGS reaction within the specified activation conditions. XRD analyses suggest that all Cr and Ce doped Fe_2O_3 fresh catalysts consist of hematite particles. Crystallite size measurements show that Fe/Cr (10:0.5) catalyst and Fe/Ce (10:2) catalyst contain smaller sized crystallites of hematite compared to the pristine hematite and other compositions. Cell parameter estimates reveal that cerium can be incorporated into hematite up to a Fe/Ce atomic ratio of 10:2. A further increase in the amount of cerium leads to demixing, i.e., a separate CeO_2 phase forms in the bulk. TPR results show that the reducibility of hematite depends on the type of the

dopant as well as the amount of dopant. TPR results also reveal that chromium acts as a structural stabilizer for the Fe_2O_3, whereas cerium promotes the reduction of hematite to magnetite. Mössbauer spectroscopy results show that the addition of both Cr and Ce replaces Fe^{2+} and Fe^{3+} ions at octahedral sites in equal amounts. These results also suggest that addition of optimal amounts of chromium and cerium to hematite stabilizes the magnetite phase during the WGS reaction. Based on the present findings, it can be concluded that the WGS activity of metal doped Fe_2O_3 depends on the type of the dopant as well as dopant concentration.

Acknowledgment. Financial support was provided by the U.S. Department of Energy (Grant DE-PS36-03GO93007). The authors also thank OCDO for providing some of the financial support.

References and Notes

(1) Kikuchi, E.; Uemiya, S.; Sato, N.; Inoue, H.; Matsuda, T. *Chem. Lett.* **1989**, 489.
(2) Lin, Y. S. *Sep. Purif. Technol.* **2001**, *25*, 39.
(3) Deng, S. G.; Lin, Y. S. *Ind. Eng. Chem. Res.* **1995**, *34*, 4063.
(4) Lin, Y. S.; Kumakiri, I.; Nair, B. N.; Alsyouri, H. *Sep. Purif. Methods* **2002**, *32*, 229.
(5) Dong, J.; Liu, W.; Lin, Y. S. *AIChE J.* **2000**, *46*, 1957.
(6) Khan, A.; Chen, P.; Boolchand, P.; Simrnitios, P. G. *J. Catal.* **2008**, *253*, 91.
(7) Costa, R. C. C.; Lelis, F.; Oliveira, L. C. A.; Fabris, J. D.; Ardisson, J. D.; Rios, R. R. A.; Silva, C. N.; Lago, R. M. *Catal. Commun.* **2003**, *4*, 525.
(8) Selim, M. S.; Turky, G.; Shouman, M. A.; El-Shobaky, G. A. *Solid State Ionics, Diffusion React.* **1999**, *120*, 173.
(9) Ramankutty, C. G.; Sugunan, S.; Thomas, B. *J. Mol. Catal.* **2002**, *187*, 105.
(10) Oliveira, L. C. A.; Rios, R. V. A.; Mussel, W. N.; Fabris, J. D.; Lago, R. M. *Stud. Surf. Sci. Catal.* **2000**, *130*, 2165.
(11) Araujo, G. C.; Rangel, M. C. *Catal. Today* **2000**, *62*, 201.
(12) Reddy, B. M.; Khan, A. *Catal. Surv. Asia* **2005**, *9*, 155.
(13) Klug, H. P. Alexander, L. E. *X-ray Diffraction Procedures for Polycrystalline and Amorphous Materials*, 2nd ed.; Wiley: New York, 1974.
(14) Shannon, R. D. *Acta Crystallogr. A* **1976**, *32*, 751.
(15) Krawitz, A. D. *Introduction to Diffraction in Materials Science and Engineering*; Wiley-Interscience: New York, 2001.
(16) Boolchand, P.; Pradhan, S.; Wu, Y.; Abdelgadir, M.; Huff, W.; Forell, D.; Coussement, R.; McDaniel, D. *Phys. Rev. B* **1992**, *45*, 921.
(17) Rhodes, C.; Hutchings, G. J.; Ward, A. M. *Catal. Today* **1995**, *23*, 43.
(18) Rhodes, C.; Williams, B. P.; King, F.; Hutchings, G. J. *Catal. Comm.* **2002**, *3*, 381.
(19) Xue, E.; O'Keeffe, M.; Ross, J. R. H. *Catal. Today* **1996**, *30*, 107.
(20) Twigg, M. V. *Catalyst Handbook*, 2nd ed.; Wolfe Publishing: London, 1989; pp 268−288.
(21) Robbins, M.; Wertheim, G. K.; Sherwood, R. C.; Buchanan, D. N. E. *J. Phys. Chem. Solids* **1971**, *32*, 717.
(22) Alonso, F. J. P.; Cabrera, I. M.; Granados, M. L.; Kapteijn, F.; Fierro, J. L. G. *J. Catal.* **2006**, *239*, 340.
(23) Lyubutin, I. S.; Lin, C. R.; Korzhetskiy, V.; Dmitrieva, T. V.; Chiang, R. K. *J. Appl. Phys.* **2009**, *106*, 034311.
(24) Reddy, B. M.; Rao, K. N.; Reddy, G. K.; Khan, A. *J. Phys Chem.C.* **2007**, *111*, 18751.
(25) Dumesic, J. A.; Tøpsoe, H. *Adv. Catal.* **1977**, *26*, 121.
(26) Edstrom, J. O. *J. Iron Steel Inst.* **1953**, *175*, 289.
(27) Sastri, M. V. C.; Vishwanath, R. P.; Vishwanath, B. *Int. J. Hydrogen Energy* **1982**, *7*, 951.
(28) Reddy, E. P.; Sun, B.; Panagiotis, P. G. *J. Phys. Chem. B* **2004**, *108*, 17198.
(29) Yuguo, Ji.; Zhao, Z.; Duan, A.; Jiang, G.; Liu, J. *J. Phys. Chem. C* **2009**, *113*, 7186.
(30) Giordano, F.; Trovarelli, A.; de Leitenburg, C.; Giona, M. *J. Catal.* **2000**, *193*, 273.
(31) Verwey, E. J. W.; Deboer, J. H. *Rev. Trav. Chim* **1936**, *55*, 531.
(32) Neel, L. *Annls. Phys.* **1948**, *3*, 137.
(33) Verwey, E. J. W.; Haayman, P. W.; Romeijn, F. C. *J. Phys. Chem.* **1947**, *15*, 181.
(34) Bauminger, R.; Cohin, S. G.; Marinov, A.; Offer, S.; Segal, E. *Phys. Rev.* **1961**, *122*, 1447.
(35) Ito, A.; Ono, K.; Iskawa, Y. *J. Phys. Soc. Jpn.* **1963**, *18*, 1465.
(36) Gotic, M.; Jurkin, T.; Music, S. *Mater. Res. Bull.* **2009**, *44*, 2014.
(37) Woude, F. V.; Sawatzky, G. A.; Morrish, A. H. *Phys. Rev.* **1968**, *167*, 533.
(38) Roca, A. G.; Marco, J. F.; Morales, M. P.; Serna, C. J. *J. Phys. Chem. C* **2007**, *111*, 18577.
(39) Wang, J.; Wu, H. Y.; Yang, C. Q.; Lin, Y. L. *Mater. Char.* **2008**, *59*, 1761.
(40) Topsoe, H.; Dumesic, J. A.; Boudart, M. *J. Catal.* **1973**, *28*, 477.
(41) Khan, A.; Smirniotis, P. G. *J. Mol. Catal. A: Chem.* **2008**, *280*, 43.

JP102959P